Theor Chem Acc (2011) 128:647–661
DOI 10.1007/s00214-010-0843-2

REGULAR ARTICLE

# Performance of density functional theory on homogeneous gold catalysis

**Olalla Nieto Faza · Roi Álvarez Rodríguez · Carlos Silva López**

Received: 19 July 2010 / Accepted: 25 October 2010 / Published online: 12 November 2010


**Abstract** The performance of 32 density functionals to describe the homogeneous gold catalysis of propargyl esters has been tested. These catalytic reactions are very commonly rather complex, numerous intermediates can be found along the reaction profile and the individual reaction steps are often associated to very small barrier heights. In this scenario, the experimental kinetic study of the catalytic mechanisms is very challenging. A computational approach to this problem provides invaluable help to gain insight into these mechanisms. However the high accuracy needed to describe such highly branched paths with low energy transition states poses many practical problems for cost-efficient DFT methods. The lack of accurate experimental or high-level computational data to employ as validation sets for these methods is also an added difficulty. High-level computational data needed to validate these functionals have been obtained at the CCSD/def2-TZVPP//CCSD/def2-SVP level and, with such data, we aim to help discern the best density functional recipe for homogeneous gold catalysis

**keywords** Gold catalysis · Density functional theory · Golden carousel

Published as part of the special issue celebrating theoretical and computational chemistry in Spain.

Ministerio de Ciencia y Innovación (CTQ2009-13703) and the Xunta de Galicia (INCITE09 314 294 PR).

**Electronic supplementary material** The online version of this article (doi:10.1007/s00214-010-0843-2) contains supplementary material, which is available to authorized users.

O. N. Faza
Departamento de Quimica Organica, Facultade de Ciencias, Universidade de Vigo, Campus as Lagoas, 32004 Ourense, Spain
e-mail: faza@uvigo.es

R. Á. Rodríguez · C. S. López (✉)
Departamento de Quimica Organica, Facultade de Quimica, Universidade de Vigo, As Lagoas (Marcosende), 36310 Vigo, Spain
e-mail: carlos.silva@uvigo.es

R. Á. Rodríguez
e-mail: roi.alvarez@uvigo.es

## 1 Introduction

The first gold-catalyzed reactions were discovered in the 70–80s. The olefin hydrogenation described by Bond et al. [1], the low-temperature oxidation of CO reported by Haruta et al. [2] or the acetylene hydrochloration to vinyl chloride of Hutchings [3], dismissed the myth of gold as a rather inert metal, without interest as a catalyst of organometallic transformations.

After these examples of heterogeneous catalysis, the description of the first asymmetric aldol reaction, using a gold(I) complex by Ito et al. [4] opened the door to the use of gold coordination compounds and salts in homogeneous catalysis, even if the exploration of this new reactivity was slow in the beginning. In 1991 Fukuda et al. expanded the use of gold to the activation of alkynes towards nucleophilic attack, using water, alcohols or amines as nucleophiles, and several years later, Teles et al. [5] continued the exploration of these catalytic systems for alcohol additions to alkynes.

After 2000, there has been a surge in the discovery and use of new gold-catalyzed reactions in organic synthesis that started with the works of Hashmi et al. expanding the use of gold catalysis to intramolecular nucleophilic additions on olefines [6, 7], their intermolecular version by Yang et al. [8]

and the comprehensive work by Echavarren et al. on enynes, highlighting the versatility of this kind of substrates in the generation of molecular complexity [9, 10].

The evolution on the field of homogeneous gold catalysis is reflected in an ever increasing number of review articles, general or restricted to a specially useful substrate [11–21]. This growing interest in gold catalysis is the result of the combination of several attractive features of these processes. Gold-catalyzed reactions usually proceed readily even under mild experimental conditions, often at room temperature, with small quantities of catalyst. In many instances, they result in the formation and/or breaking of several bonds in a one-pot reaction, achieving high atom efficiency and reducing waste. The easy generation of complexity and the compatibility with a wide range of functional groups make these reactions versatile alternatives to more conventional synthetic approaches and allow transformations not available with other catalysts.

At the root of many of these features are the unusual properties of gold, sometimes surprisingly different from those of neighboring elements in the periodic table or other transition metals. Among these properties are its yellow color, small metallic radius, high ionization potential and an associated high electronegativity, high electron affinity and aurophilicity [22]. Relativistic effects need to be invoked to explain these properties [23]. Thus, the contraction of the 6*s* orbital lowers the LUMO energy and leads to larger ionization potentials, stronger ligand-metal bonds and higher acidity, while the expansion of the *d* and *f* orbitals due to the larger shielding of the contracted core makes this metal softer and less nucleophilic [24].

These properties set gold's catalytic activity apart from that of the most studied transition metals, making it less prone to the oxidative addition/reductive elimination cycles common with other metals. There are studies where a careful functionalization of the substrate leads to a multifaceted character of gold, with the metal playing a different role at different stages of the catalytic cycle [25], and others where the metal center changes its oxidation state along a gold-catalyzed cross-coupling [26, 27], but most of the described gold-catalyzed reactions use its properties as a $\pi$-acid, activating unsaturated compounds towards nucleophilic attack.

The impressive diversity and complexity of the reactions available to a gold-activated unsaturation creates the need for mechanistic information on the reaction paths available and their relative energies if predictive power and systematization and optimization of these transformations are sought. However, the short lifespan of many of the intermediates in the catalytic cycles (which makes their characterization difficult) and the ramifications in the more complex reaction paths make the experimental study of these mechanisms a difficult task. Molecular modeling steps in at this stage, allowing the chemist to differentiate between competitive reaction mechanisms, to characterize intermediates or simply to provide a step-by-step description of the structural and energy changes along the reaction path. Synergy between theory and experiment has already been successful in the characterization and systematization of such reaction mechanisms and its relevance in the future is predicted to increase [28–30].

The extensive reviews on computational chemistry of gold by Pyykkö [31–33] compile an impressive amount of information about the computational approaches used to describe different properties of gold and its compounds. Special attention is devoted to the relativistic origin of gold's more characteristic behaviors and to the techniques used to reproduce oxidation states, coordination number and structure in different complexes, gold's behavior as a proton or halide analogue, aurophilicity, spectroscopy, etc. However, there is not much information on the organometallic compounds generated as intermediates in the homogeneous catalytic cycles of interest to organic chemists, and even less on the properties of the transition structures that connect these intermediates. This owes probably to one of the reasons why gold-catalysis is so attractive: the speed of these reactions in mild conditions, which makes difficult the isolation and characterization of intermediates resulting in a dearth of experimental data against which to compare the results of computational models. Other works, such as those of Pernpointner et al. [34], or Lein et al. [35] also highlight the need to use relativistic calculations in order to correctly describe gold complexes.

Very useful reviews for those interested in modeling organometallic mechanisms have appeared of late [36–39], evaluating the different options available and describing the latest advances. Many of the conclusions of these works can be applied to gold-catalyzed mechanisms, however, they are general in scope and don't directly address the special features of gold or, when doing so, tend to focus in gold clusters or complexes rather than mechanisms in homogeneous gold catalysis [40].

In most computational studies of gold-catalyzed mechanisms, the method of choice is based in Density Functional Theory (DFT) [41], which includes some correlation at a moderate computational cost. The most popular functional by far (as in other computational endeavors in organic chemistry) is B3LYP [42, 43] with 6–31G(d) as the most common basis set for the main group atoms and a pseudopotential (ECP) and the associated basis for the metal atom.

Electron core potentials are used in these calculations with two aims: reducing the computational cost associated to the large number of core electrons in gold and, most importantly, parametrically incorporating part of the

relativistic effects. Among the most commonly used ECPs in gold-catalyzed organic reaction mechanisms are LANL2DZ [44] or SDD [45]. In the most recent works, however, the need to attain more accurate results, led to the use of somewhat larger basis (triple-ζ with polarization and diffuse functions) for geometry optimizations or, at least in single point energy refinements. The success of new generation functionals such as M06 in organometallic catalysis and the development of new basis functions and pseudopotentials opens the door to a better description of these complex mechanisms and further modeling achievements [46].

There is ample work on the development and application of methodologies for the modeling of gold chemistry, but it is not directly focused on reaction mechanisms and thus not very accessible to the computational organic chemist. Thus, in most of the work published on modeling homogeneous gold catalysis, the choice of method is usually supported by some calculations on model systems and/or the agreement of the conclusions of the study with the bench results, without any further validation. This approach is oftentimes satisfactory, since small variations between methods in reaction energies and barriers don't always affect the preferred reaction paths or a qualitative description of the mechanism. However, there are many instances of different competitive reaction paths in a narrow energy bracket where small errors can lead to a dramatic reversal of product distributions. An example of that could be the paper by Benítez et al. where the authors show that M06 is able to reproduce the effect of the donor properties of gold's ligand on the experimental barriers for bond rotation in gold carbenoids, while other functionals (B3LYP or BP86) can not [47].

### 1.1 Choice of model system

From the great variability found in gold-catalyzed reactions, some quite general reactivity patterns have emerged as a result of the combination of theoretical and experimental mechanistic studies. Among them, those corresponding to enynes and propargylic esters are specially relevant. In these mechanisms, the extra delocalization of the expanded 5*d* orbitals generates a series of carbocationic or carbenoid intermediates which can be the starting point of complex cascade reactions or reorganizations. In this work, we will focus on the gold-catalyzed reactivity of propargyl esters, where the combination of an alkyne and a bidentate internal nucleophile can open a wealth of reaction paths well described in many publications [48–50]. For this, we will use the *golden carousel* of Correa et al. as a template [48], a clever representation of these available paths that clearly showcases the three main paradigms of reactivity in which these systems can be involved: π-activated unsaturations, carbenoid/carbocation reactivity and allene chemistry. This structural variety in the intermediates and transition structures is specially interesting in the assessment the robustness of a computational methodology (it constitutes a real challenge for some of the methods) and covers a wide range of organic gold reactivity.

In order to evaluate a broad combination of methods and, at the same time, being able to produce high quality reference results, we decided to simplify the organic substrate to a simple propargylic acetate and the catalyst to gold with the simplest phosphine, $PH_3$, as a ligand. With this model we are able to compute coupled-cluster level geometries and energies as references. Effects of the introduction of more complexity on both the substrate and the catalyst will be studied after the performance of the different density functionals is known for the model system.

The mechanism studied is thus depicted in Fig. 1. From the propargyl ester-gold complex **2**, there are two paths available, a *1,2-migration* involving a nucleophilic attack of the carbonyl oxygen to the alkyne proximal carbon and a *1,3-migration* involving the same kind of attack onto the alkyne terminal position. A cyclic intermediate (**3** or **5**) is formed in the two paths, which undergoes the cleavage of the original C–O resulting in the first case in a gold-carbenoid/carbocationic species (**4**) and in the second in a gold-coordinated allene (**6**). The latter intermediates can be connected by a second *1,2-migration* on **6** to yield **8**, which converts to **4** through a low-energy rotation of the ester group. For some of the transformations in the mechanism, the bond-forming processes can take place on the same or opposite side of gold, for what we have used the descriptors *syn* and *anti*, respectively.

## 2 Computational methods

### 2.1 Density functionals

Density functional theory is nowadays amongst the most widely employed electronic structure models for molecular simulations. This methodology combines the benefits of the low computational cost of single determinant models with the recovery of electron correlation comparable to higher order and more costly *ab-initio* methods. However, given the tremendous effort put forward by developers in the last decades, the bouquet of different functionals has grown to an unpractical size. It is, therefore, not unlikely that computational chemists are drawn into the daunting discussion on whether their work should have better been addressed with whatever the favorite functional is for the inquirer. Last developments in several fronts (perturbatively

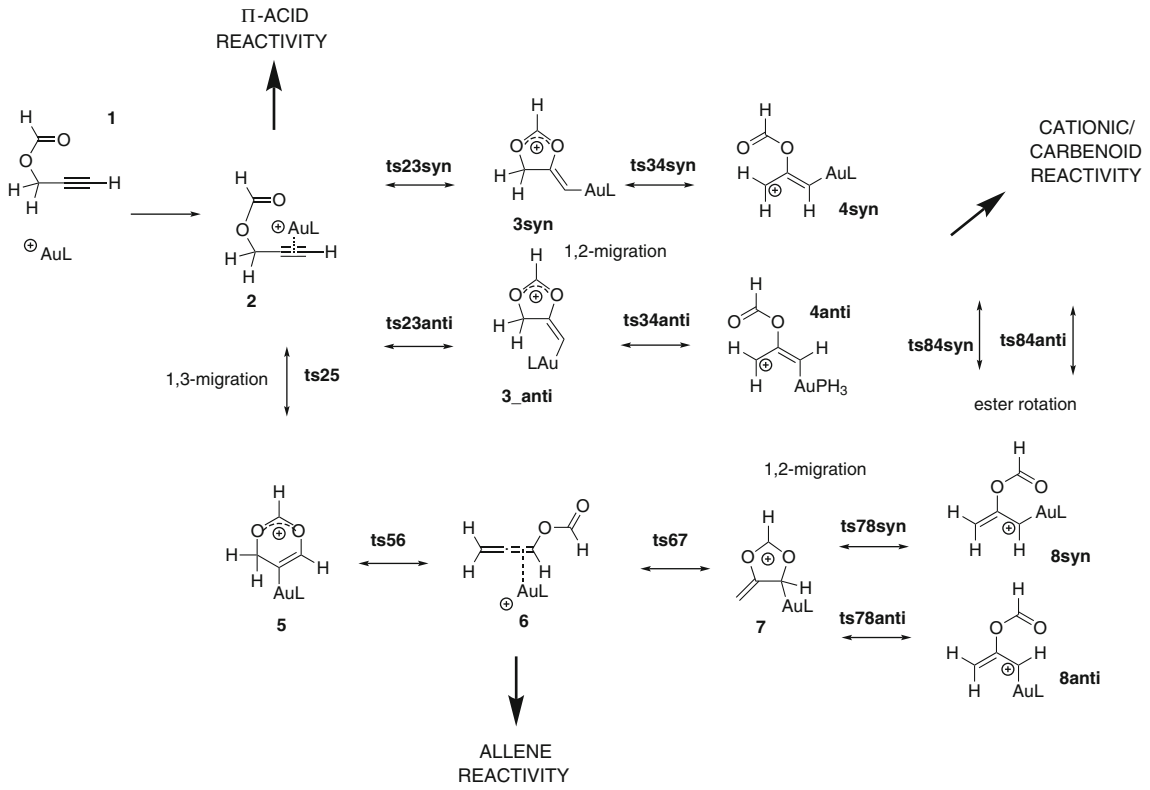


**Fig. 1** A simplified model of the *gold-carousel* of Correa et al. [48]. The stationary points depicted in this Scheme will be used to benchmark the performance of different computational methods, specially focusing on DFT

corrections, long-range corrections, empirical dispersion terms, meta-hybrids, etc) in the pursuit for the *divine functional* [51] have proved to provide remarkable improvements over popular choices, but have also shed more arguments to be added to the functional discussion. This situation, despite being obviously positive in terms of number of choices, is less than ideal due to the lack of a broadly recognized standard. Hot, new topics, like gold organocatalytic chemistry, suffer a particular overexposure to this problem, since very few comprehensive benchmarks include organometallic species in their datasets. Even if this subject is gaining interest [52–54], these studies are usually limited to the first period of transition metals, and less often include second row transition metal [36, 40, 52], and, to our knowledge, none include organo-gold catalytic chemistry.

At this juncture, we aim to provide a thorough comparison on the performance of a large number of density functionals to model the *golden carousel* [48]. In this benchmark work we have included 32 density functionals that should represent all the generations included in Perdew's ladder (see Table 1) [55]. All the functionals have been compared to purposely generated coupled cluster reference data. To the series of density functionals, and for the sake of historical completeness, the *ab-initio* Hartree–Fock (HF) theory and Möller–Plesset second order (MP2) perturbation theory have been included in this test set.

In Perdew's ladder of density functional development, the strategy aimed to keep into each next generation of functionals everything that was working and add on top of that new improvements for what was not. In this scenario the different generations of functionals can be classified analogously in terms of chronological history or degree of sophistication:

LDA: Local Density Approximation is the simplest and earliest density functional model. It stems directly from solid state physics and is based in the solution to the homogeneous electron gas [56, 80, 81]. Given the physical model from which LDA is derived it is surprising that it performs decently well for molecular systems. It is obvious that the electron density of molecules is far from homogeneous, however, LDA does predict correct geometries and energies for systems with slowly varying charge densities. The relative success of this approximation has been suggested to depend on the cancellation of errors [82].

GGA: The natural step further from LDA is to account for the non-homogeneity of the electron density in molecular systems. Thus in the Generalized

**Table 1** Density functionals and ab-initio methods included in the benchmark

| ab-initio | LDA | GGA | meta-GGA | Hybrid | Dispersion corrected[a] |
|---|---|---|---|---|---|
| HF | SVWN [56] | mPWLYP [43, 57] | M06L [58] | TPSSh [59] | M06 [60] |
| MP2 | | mPWPBE [57, 61] | VSXC [62] | $\tau$-HCTHhyb [63] | $\omega$B97 [64] |
| | | mPWPW91 [57, 65] | TPSS [59] | mPW1LYP [43, 57] | cam-B3LYP [66] |
| | | OLYP [67] | $\tau$-HCTH [63] | mPW1PW91 [57, 65] | LC-$\omega$PBE [68] |
| | | BLYP [43, 69] | BB95 [69, 70] | mPW3PBE [57, 61] | LC-BLYP [43, 69, 71] |
| | | BPW91 [65, 69] | PBEKCIS [61, 72] | O3LYP [73] | B2PLYP [74] |
| | | PBEPBE [61] | | B1B95 [70, 75] | |
| | | HCTH [76] | | B3LYP [42, 43, 77] | |
| | | | | B3PW91 [42, 65] | |
| | | | | PBE1KCIS [72, 78] | |
| | | | | PBEh1PBE [79] | |

[a] In this column the new generations of perturbatibely and empirically corrected functionals and Coulomb-attenuated hybrids and GGA functionals are included

Gradient Approximation the exchange-correlation functional form adopts dependency on both the value of the density and its gradient [65, 83]. The inclusion of the first derivatives of the electron density in the description of density functionals leads to significant improvements. A wealth of different functionals were developed under the auspices of the GGA model (see Table 1 for a few popular examples). The Generalized Gradient Approximation was probably one of the main reasons for the wide spread of Density Functional Theory in chemistry during the 1990's.

meta-GGA: The next rung in Perdew's ladder involves the recent development of functionals in which an extra ingredient is added to the GGA recipe. In this generation explicit dependency on the Laplacian of the spin density or on the Kohn-Sham orbital kinetic energy density is included into the functionals [62, 84, 85].

Hybrid: Hybrid functionals include a mixture of exact exchange derived from Hartree–Fock theory. This addition was originally justified in terms of the dramatic improvements in atomization energies of molecules [70]. Loosely bound structures are not well described by local and GGA approaches due to the self-interaction error [86]. The inclusion of exact exchange therefore also improves the performance of functionals in chemical kinetics since transition states in particular are prone to be overstabilized by LDA and GGA methodologies. The need for exact exchange in DFT is however questioned [87] on the grounds that new self-interaction correction schemes are capable of improving energy barriers [88].

In this already complex scenario of density functionals, the approaches to further improve these methods are unfortunately diverging. The density functionals described above are known to still lack an accurate description of the dispersion energy, so strategies to overcome this limitation have been proposed resulting in the apparition of several successful density functionals that generally offer improved performance for difficult systems where non-convalent interactions are important. Following the order shown in Table 1 we find the following strategies:

M06: The series of new Minnesota functionals by Truhlar and coworkers have been built with a specific purpose in mind. This is exemplified by Truhlar himself with the metaphoric carpenter who needs different tools for different tasks. Following these guideline it is not surprising that the M06 series have been obtained after a thoughtful selection of parametrization datasets, several of which are dedicated to weak, dispersion-like, non-bonding interactions [89].

$\omega$B97 Long-range interactions are commonly wrongly described by GGA and hybrid functionals. Chai and Head-Gordon developed a partitioning scheme based on the standard error function that separates short- and long-range regions and applied density functional theory to the former, whereas 100% of the exact-exchange is computed for the latter. With this approach $\omega$B97 proves superior performance for problematic systems, like charge transfer interactions, $\pi$-stacking, and other interactions sensitive to the self-interaction errors [64].

cam-

B3LYP Handy and coworkers aim to improve the known deficiencies of the popular B3LYP functional by applying a long-range correction that switches from 0.19 Hartree–Fock plus 0.81 Becke 1988 (B88) exchange at short range with 0.65 HF and 0.35 B88 at long-range. The medium-range smooth switching function in this case is also based on a standard error function [66].

LC-

$\omega$PBE Vydrov and Scuseria find that the application of a long-range correction scheme to the PBE functional results in a particularly well performing combination. To construct LC-$\omega$PBE these authors also rely on splitting the short- and long-range regions through a standard error function [68].

LC-

BLYP Hirao and coworkers aim to apply a similar correction to GGA functionals. However, the common correction scheme is unpractical with these functionals due to the lack of first-order density matrices. In their work they therefore propose a long-range correction strategy based on constructing approximated first-order density matrices [71]. Often times this scheme is applied to the BLYP GGA functional, as in this work, but Hirao's approach is general and can be applicable to any GGA functional.

B2PLYP Grimme has explored the idea of going a step further into the successful history of hybrid functionals by, not only admixing a portion of the exact Hartree–Fock exchange to density functionals, but also adding a perturbative correction obtained through the Kohn-Sham orbitals. This approach has been termed double hybrid and, in one of the most successful functionals so constructed (B2PLYP) it only implies two parameters that determine the amount of HF and GGA exchange on the one side and the GGA and PT2 correlation on the other. These parameters have been obtained by a least-squares-fit procedure to the G2/97 set of heat of formations. B2PLYP is claimed to be one of the best general purpose density functional for molecules [74]. The only drawback for this otherwise promising functional is the cost associated to the perturbative correction, which places it among the most computationally demanding functionals to date.

## 2.2 Methodology

All density functional optimizations in this work have been performed with the Gaussian09 electronic structure package [90]. In most calculations we used the default values of Gaussian09 for convergence thresholds. A finer integration grid containing 99 radial shells and 590 angular points per shell, however, has been employed throughout the entire study (see below). Such finer grid is needed for two purposes: to avoid spurious imaginary frequencies in the calculation of second derivatives, and to correctly integrate the kinetic-energy dependent functionals [91]. Of note here is our intent to propose a general protocol that can be use with certain confidence by the organic chemist in the modeling of gold-catalyzed reactions, so we try, where possible, to minimize the fine tuning of the programs options. The density functionals have been accompanied by the large double-$\zeta$ quality basis set def2-SVP [92]. Relativistic effects have been introduced through electron core potentials associated with these series of basis sets [93]. The stability of the wavefunction has been computed for all stationary points [94]. The nature (minimum or transition state) of each stationary point has been determined through harmonic analysis of the second derivatives of the energy with respect to the nuclear displacements.

The performance of electron core potentials to describe relativistic effects has also been compared with all electron calculations with the Douglas-Kroll-Hess second order scalar relativistic model [95, 96].

### 2.2.1 *Integration grid*

As mentioned earlier, a very dense grid has been employed for the numerical integration of density functionals. A side study on the convergence of single point energies with the M06 functional with respect to the grid size has been performed on the reference geometries of all the stationary points using the standard basis set and ECP. The resultant profiles are shown in Fig. 2, where absolute electronic energies are noted in kcal/mol. It can be seen that while

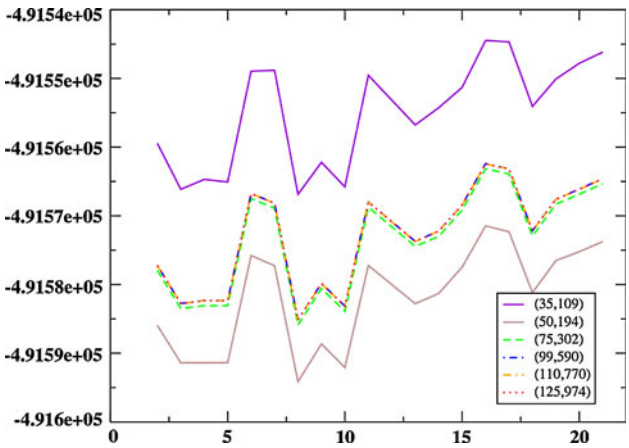


**Fig. 2** Energy convergence (kcal/mol) of M06/def2-svp,ecp60mwb single point calculations with respect to integration grid size

sparser grids, such as the (35,110) or (50,194) corresponding to the "coarse" denomination in Gaussian09 and to the "SG1" (standard grid 1) [97], respectively, are not converged, the "fine" grid (75,302) yields almost converged results. The energies computed with the "ultrafine" grid we used in all the calculations (99,590) being almost indistinguishable from the values obtained for the two largest grids: (110,770) and (125,974), we can safely assume therefore that the energies computed with these functionals are converged with respect to the grid size of the numerical integration scheme.

### 2.3 Reference data

Highly accurate reference data for this benchmark study have been obtained through the coupled-cluster multideterminant methodology. CCSD optimizations have been performed on previously DFT optimized structures. For these optimizations we have also employed the def2-SVP basis set. Energy refinements have been carried out by expanding the basis set to the triple-$\zeta$ quality and strongly polarized def2-TZVPP [98] and are noted CCSD/def2-TZVPP//CCSD/def2-SVP.

## 3 Results and discussion

### 3.1 Geometries

Optimized geometries have been obtained for HF, MP2 and the 32 functionals included in this work, and they have been compared with reference structures computed at the CCSD/def2-SVP level. This comparison has been carried out in a sequential strategy: first, backbone bond-lengths have been analyzed and compared to reference structures to account for deviations in different types of *bonding interactions*; second, bond angles have been studied in a similar manner to account for errors in *short-range* non-bonding interactions; finally, the overall RMS fit of the structure backbones with that of the reference has been obtained. The study of these three geometric parameters should give a good assessment of the quality of the geometries for these methods.[1]

The performance of density functional theory with main group atom chemistry (geometries, energetics, etc) is usually covered very thoroughly in the development of each functional form, we will therefore focus our attention more on the specific parameters where gold chemistry is involved. The results summarized in Table 2 indicate that, in general, all density functionals perform reasonably well with bond lengths. The errors obtained are usually contained to less than 0.02 Å when gold is involved and less than 0.01 Å for C–C and C–O bonds. The bond lengths computed with HF theory and LDA are considerably worse than those obtained with the rest of density functionals. Both show outliers with very large errors (0.19 and 0.11 Å for C–Au and Au–P in HF, and 0.15 and 0.07 Å in SVWN, respectively) and considerably sparse distributions with respect to the reference. MP2 shows a dual behavior performing remarkably well for C–C and C–O bonds and quite poorly for gold containing bonds. A systematic improvement of the bond description as we move up in the sophistication of the density functionals is observed; however, in general, this improvement affects more dramatically the strength of the correlation (smaller standard deviations) than the mean errors. This trend also affects the maximum absolute deviations, which are considerably reduced when stepping from GGA and meta-GGA functionals to their hybrids and dispersion corrected forms. The performance of the double hybrid functional by Grimme is excellent in this area, providing very low mean errors and narrow standard deviations across the table. M06L also stands out of the meta-GGA set, showing a level or performance on par with most hybrids. On the contrary, the long-range corrected functionals LC-BLYP and LC-$\omega$PBE offer inferior results than their counterparts, particularly for the gold-containing bonds, and, in general, they significantly overbind all systems.

Similar statistics were performed on the backbone $\widehat{CCC}$ and $\widehat{AuCC}$ angles which we considered the most relevant in terms of the gold catalytic process. There is some controversy on whether some organogold intermediates responsible for alkyne bond activation are carbenium ions (in which the gold would be acting as a very soft Pearson acid) or gold carbenes (in which double bond character and retrodonation would be expected for the C–Au interaction). In this scenario, the accurate description of both the $\widehat{AuCC}$ and the carbon backbone is key to cement solid knowledge on the nature of these Au–C interactions.

The different generations of functionals sampled also show systematic improved performance in the description of these bond angles when moving upwards in Perdew's ladder (see Table 3). LDA offers very poor results for this geometric parameters. GGA and meta-GGA functionals perform better although their outliers show large deviations (15–18 degrees) and the stardard deviation values suggest a broad variability. Again, the biggest step towards improving the accuracy is introducing exact exchange in this functional forms. Hybrid functionals, therefore, show standard deviations reduced by 50% with respect to most GGA and meta-GGA approaches. Dispersion corrected

[1] Statistical analysis has been carried out on the molecular backbone (i.e. neglecting the hydrogen atoms) to avoid artifactual errors due to the soft normal mode of the phosphine rotation.

**Table 2** Statistical analysis (mean error, standard deviation and maximum absolute error) of the bond-lenghts obtained with HF, MP2 and the 32 density functionals included in this work (data in $\text{Å} \cdot 10^2$)

| Method | C–C | | | C–O | | | C–Au | | | Au–P | | |
|---|---|---|---|---|---|---|---|---|---|---|---|---|
| | $\overline{\epsilon}$ | $\sigma_{\overline{\epsilon}}$ | MAD | $\overline{\epsilon}$ | $\sigma_{\overline{\epsilon}}$ | MAD | $\overline{\epsilon}$ | $\sigma_{\overline{\epsilon}}$ | MAD | $\overline{\epsilon}$ | $\sigma_{\overline{\epsilon}}$ | MAD |
| ab initio | | | | | | | | | | | | |
| HF | −1.1 | 1.2 | 3.1 | −2.0 | 0.8 | 3.4 | 7.4 | 4.2 | 19.3 | 5.6 | 1.8 | 11.4 |
| MP2 | −0.1 | 0.7 | 1.6 | 0.3 | 0.5 | 1.1 | −4.3 | 2.1 | 10.9 | −3.9 | 0.5 | 5.0 |
| LDA | | | | | | | | | | | | |
| SVWN | −1.3 | 1.3 | 3.9 | −0.9 | 1.4 | 3.5 | −4.5 | 4.1 | 15.4 | −5.3 | 1.1 | 7.2 |
| GGA | | | | | | | | | | | | |
| HCTH | −0.5 | 0.9 | 3.2 | 0.1 | 0.7 | 2.1 | −0.3 | 2.5 | 6.3 | −1.0 | 0.8 | 2.2 |
| PBEPBE | 0.1 | 1.0 | 2.2 | 1.1 | 0.7 | 3.5 | −1.5 | 2.2 | 7.2 | −0.7 | 0.8 | 2.3 |
| BPW91 | 0.1 | 1.0 | 2.1 | 1.2 | 0.7 | 3.8 | −0.9 | 2.2 | 6.8 | −0.3 | 0.8 | 2.0 |
| BLYP | 0.4 | 0.9 | 2.0 | 2.0 | 1.1 | 4.9 | 2.0 | 3.1 | 10.4 | 2.7 | 0.8 | 3.8 |
| OLYP | 0.1 | 0.9 | 2.5 | 0.8 | 0.8 | 3.2 | −0.4 | 2.8 | 7.1 | −0.3 | 0.9 | 1.8 |
| mPWPW91 | 0.0 | 1.0 | 2.1 | 1.1 | 0.7 | 3.6 | −1.1 | 2.1 | 6.8 | −0.5 | 0.8 | 2.1 |
| mPWPBE | 0.1 | 1.0 | 2.2 | 1.1 | 0.7 | 3.6 | −1.4 | 2.2 | 7.2 | −0.7 | 0.8 | 2.4 |
| mPWLYP | 0.3 | 0.9 | 1.9 | 1.9 | 1.0 | 4.7 | 1.8 | 2.8 | 9.3 | 2.5 | 0.7 | 3.6 |
| Meta-GGA | | | | | | | | | | | | |
| PBEKCIS | 0.1 | 1.0 | 2.5 | 1.2 | 0.7 | 3.8 | −0.5 | 2.1 | 6.3 | −0.1 | 0.8 | 1.4 |
| BB95 | 0.0 | 1.0 | 2.2 | 1.2 | 0.6 | 3.3 | −1.2 | 2.0 | 6.7 | −0.6 | 0.9 | 2.6 |
| $\tau$-HCTH | −0.4 | 0.9 | 2.7 | 0.3 | 0.7 | 2.8 | −0.6 | 2.4 | 6.2 | −1.8 | 0.7 | 3.0 |
| TPSSTPSS | 0.0 | 0.8 | 1.7 | 1.2 | 0.7 | 3.3 | −0.8 | 2.3 | 6.2 | −0.4 | 0.9 | 2.2 |
| VSXC | 0.0 | 0.6 | 1.5 | 1.1 | 1.1 | 3.8 | 1.7 | 2.2 | 9.9 | 1.6 | 0.9 | 2.9 |
| M06L | −0.9 | 0.8 | 3.0 | 0.0 | 0.6 | 1.6 | 0.3 | 1.5 | 4.6 | 0.2 | 0.7 | 1.3 |
| Hybrid | | | | | | | | | | | | |
| PBEh1PBE | −0.8 | 0.6 | 2.2 | −0.6 | 0.4 | 1.9 | −1.1 | 1.5 | 5.4 | −1.3 | 0.6 | 2.1 |
| PBE1KCIS | −0.7 | 0.7 | 2.4 | −0.4 | 0.4 | 1.7 | −0.6 | 1.4 | 5.1 | −1.0 | 0.5 | 1.7 |
| B3PW91 | −0.7 | 0.6 | 2.2 | −0.3 | 0.4 | 1.4 | −1.0 | 1.5 | 5.6 | −1.1 | 0.6 | 1.8 |
| B3LYP | −0.5 | 0.5 | 1.8 | 0.2 | 0.5 | 1.2 | 1.2 | 1.5 | 4.3 | 1.1 | 0.3 | 1.8 |
| B1B95 | −1.0 | 0.5 | 2.2 | −0.8 | 0.4 | 2.3 | −1.2 | 1.6 | 5.4 | −1.8 | 0.5 | 2.5 |
| O3LYP | −0.4 | 0.7 | 2.4 | 0.0 | 0.5 | 1.4 | −0.4 | 2.0 | 6.0 | −0.6 | 0.7 | 1.5 |
| mPW3PBE | −0.7 | 0.7 | 2.2 | −0.4 | 0.4 | 1.6 | −1.3 | 1.6 | 6.0 | −1.4 | 0.6 | 2.2 |
| mPW1PW91 | −0.8 | 0.6 | 2.2 | −0.6 | 0.4 | 1.8 | −1.1 | 1.5 | 5.5 | −1.4 | 0.6 | 2.2 |
| mPW1LYP | −0.5 | 0.5 | 1.6 | 0.0 | 0.4 | 0.9 | 1.5 | 1.4 | 5.1 | 1.3 | 0.3 | 1.9 |
| Dispersion-corrected | | | | | | | | | | | | |
| $\tau$-HCTHhyb | −0.2 | 0.7 | 1.7 | 0.1 | 0.5 | 1.9 | −0.8 | 1.7 | 5.4 | −0.5 | 0.5 | 1.2 |
| TPSSh | −0.4 | 0.7 | 1.8 | 0.5 | 0.5 | 2.1 | −0.9 | 2.0 | 5.8 | −0.8 | 0.7 | 1.8 |
| B2PLYP | −0.3 | 0.4 | 1.1 | 0.3 | 0.3 | 1.0 | −0.4 | 1.0 | 3.1 | −0.5 | 0.3 | 1.0 |
| LC-BLYP | −1.7 | 0.5 | 2.8 | −1.4 | 0.6 | 2.8 | −2.2 | 2.3 | 9.6 | −2.8 | 0.8 | 3.5 |
| LC-$\omega$PBE | −1.1 | 0.5 | 2.1 | −0.8 | 0.5 | 2.0 | −1.9 | 2.6 | 9.3 | −2.5 | 0.9 | 3.6 |
| cam-B3LYP | −0.9 | 0.4 | 1.9 | −0.5 | 0.3 | 1.3 | 0.0 | 1.0 | 2.9 | −0.4 | 0.5 | 1.0 |
| $\omega$B97 | −0.5 | 0.4 | 1.3 | −0.1 | 0.3 | 1.0 | 0.0 | 1.7 | 4.9 | −0.9 | 0.9 | 1.7 |
| M06 | −0.9 | 0.5 | 2.3 | −0.5 | 0.4 | 1.6 | 1.5 | 1.2 | 3.6 | 2.3 | 0.5 | 3.5 |

forms provide, in general, the best results compared to our CCSD reference. Within the GGA and meta-GGA group M06L and VSXC stand out for their good description of these bond angles, both functionals offer smaller errors than directly compete or better those obtained from hybrid alternatives. Again, the best overall results are obtained with the double hybrid by Grimme although $\omega$B97 and M06 are very close behind.

A similar picture of the performance of the series of functionals included in this studied is obtained when

**Table 3** Statistical analysis (mean error, standard deviation and maximum absolute error) of the $\widehat{CCC}$ and $\widehat{AuCC}$ bond-angles obtained with HF, MP2 and the 32 density functionals included in this work (in degrees)

| Method | $\widehat{CCC}$ | | | $\widehat{AuCC}$ | | |
|---|---|---|---|---|---|---|
| | $\bar{\epsilon}$ | $\sigma_{\bar{\epsilon}}$ | MAD | $\bar{\epsilon}$ | $\sigma_{\bar{\epsilon}}$ | MAD |
| ab initio | | | | | | |
| HF | 0.4 | 1.6 | 4.8 | 2.6 | 2.5 | 8.7 |
| MP2 | −0.8 | 1.2 | 3.6 | −1.5 | 1.5 | 5.5 |
| LDA | | | | | | |
| SVWN | 3.2 | 5.7 | 17.9 | −3.6 | 8.9 | 25.4 |
| GGA | | | | | | |
| HCTH | 1.2 | 3.6 | 12.4 | 1.2 | 2.5 | 5.8 |
| PBEPBE | 2.0 | 4.5 | 17.3 | −0.5 | 5.0 | 18.1 |
| BPW91 | 2.0 | 4.6 | 17.2 | −0.2 | 4.7 | 16.7 |
| BLYP | 2.3 | 4.9 | 18.4 | 0.3 | 4.6 | 15.7 |
| OLYP | 1.4 | 4.1 | 14.3 | 1.1 | 3.1 | 8.1 |
| mPWPW91 | 2.1 | 4.6 | 17.4 | −0.4 | 4.9 | 17.6 |
| mPWPBE | 2.0 | 4.6 | 17.4 | −0.4 | 5.0 | 17.8 |
| mPWLYP | 2.3 | 4.8 | 18.5 | 0.1 | 4.7 | 16.5 |
| Meta-GGA | | | | | | |
| PBEKCIS | 1.9 | 4.4 | 17.1 | 0.1 | 4.4 | 15.7 |
| BB95 | 1.8 | 4.0 | 15.7 | −0.4 | 4.4 | 16.1 |
| $\tau$-HCTH | 1.8 | 4.5 | 16.3 | 0.4 | 4.2 | 14.1 |
| TPSSTPSS | 2.1 | 4.3 | 16.2 | −0.6 | 5.0 | 17.7 |
| VSXC | 1.0 | 3.3 | 7.2 | −2.5 | 2.4 | 7.0 |
| M06L | 1.0 | 1.7 | 4.7 | 1.1 | 1.4 | 4.7 |
| Hybrid | | | | | | |
| PBEh1PBE | 1.0 | 2.4 | 8.4 | 0.2 | 2.3 | 6.5 |
| PBE1KCIS | 0.9 | 2.3 | 7.8 | 0.8 | 1.7 | 5.5 |
| B3PW91 | 1.2 | 2.7 | 9.6 | 0.4 | 2.4 | 6.6 |
| B3LYP | 1.2 | 2.3 | 7.6 | 1.0 | 1.6 | 5.1 |
| B1B95 | 0.7 | 1.7 | 5.8 | 0.3 | 1.7 | 4.9 |
| O3LYP | 1.0 | 2.9 | 9.3 | 1.3 | 1.9 | 5.1 |
| mPW3PBE | 1.2 | 2.8 | 10.0 | 0.2 | 2.7 | 7.9 |
| mPW1PW91 | 1.1 | 2.4 | 8.5 | 0.4 | 2.3 | 6.1 |
| mPW1LYP | 1.1 | 1.9 | 6.0 | 1.1 | 1.3 | 4.5 |
| Dispersion-corrected | | | | | | |
| $\tau$-HCTHhyb | 1.5 | 3.4 | 12.4 | 0.0 | 3.2 | 10.4 |
| TPSSh | 1.6 | 3.3 | 12.3 | −0.2 | 3.8 | 12.6 |
| B2PLYP | 0.5 | 1.4 | 3.3 | 0.2 | 1.1 | 3.0 |
| LC-BLYP | 1.0 | 2.1 | 6.0 | 0.4 | 2.2 | 5.3 |
| LC-$\omega$PBE | 0.7 | 1.9 | 5.8 | 0.2 | 2.3 | 5.4 |
| cam-B3LYP | 1.1 | 1.8 | 6.2 | 0.8 | 1.4 | 4.8 |
| $\omega$B97 | 0.8 | 1.4 | 4.4 | 0.4 | 1.2 | 3.5 |
| M06 | 0.9 | 1.4 | 4.1 | 0.8 | 1.1 | 3.5 |

carrying out a RMS fitting procedure of each structure with its reference (see Fig. 3). The geometries of the stationary points in the *gold carousel* reaction mechanism improve as we move towards more sophisticated functionals. Again, the M06L functional stands out of the GGA and meta-GGA families performing considerably better than any other functional in this set and also improving the results offered by many hybrid counterparts. The best two functionals in this arena are B2PLYP which provides very small errors across the entire mechanism, and M06, displaying errors consistently below 0.05 Å with respect to the CCSD geometries at a fraction of the computational cost.

It is worth noting that the errors are not evenly distributed along the stationary points in the mechanism. Several structures prove to be very difficult for entire families of density functionals. Among them, transition states **TS-23-anti**, **TS-23-syn** and **TS-25** seem to be the most challenging. Errors are somehow smaller when reproducing structures related to energy minima than transition states, particularly of GGA and meta-GGA. However, some minima do seem problematic for various hybrid functionals (see, for instance, **4-anti** and **4-syn**), and, quite unexpectedly, the structurally simple and non-gold-containing propargylic esther **1** is the most challenging minimum in this mechanism. This is probably due to the very soft mode of rotation about the C–C simple bond (See Fig. 4).

### 3.2 Energy profiles

A fitting procedure based on RMS deviations from a high-level coupled-cluster based reference has also been carried out for the relative energies of the stationary points describing the *golden carousel*. It is surprising how Hartree–Fock theory and its second order perturbation correction afforded fairly reasonable geometries, as described above, and also provide relative energies with errors that are smaller than those of all GGA and most meta-GGA functionals. Only hybrid functionals, which, in fact, include a fraction of the Hartree–Fock exchange, improve the RMS values of HF and MP2. Furthermore, only the dispersion corrected formulations consistently show smaller maximum deviations than MP2.

In terms of the energy profiles the M06L meta-GGA formulation by Truhlar provides results on par with most hybrids, and at the same time offer better size-scaling conditions for more complex systems. B1B95 also performs better than its counterparts and exhibits a very contained MAD of 3.7 kcal/mol. Actually, this functional does perform quite accurately as well in terms of the geometric parameters, the only reason for B1B95 to not be mentioned in Sect. 3.1 is that it considerably overbinds all the stationary points included in this work (see Table 2). The best performing functionals are found again among the dispersion-corrected set. B2PLYP, M06 and $\omega$B97 provide relative energy profiles with maximum deviations smaller than 3 kcal/mol and RMS contained to less than 1.7 kcal/mol.

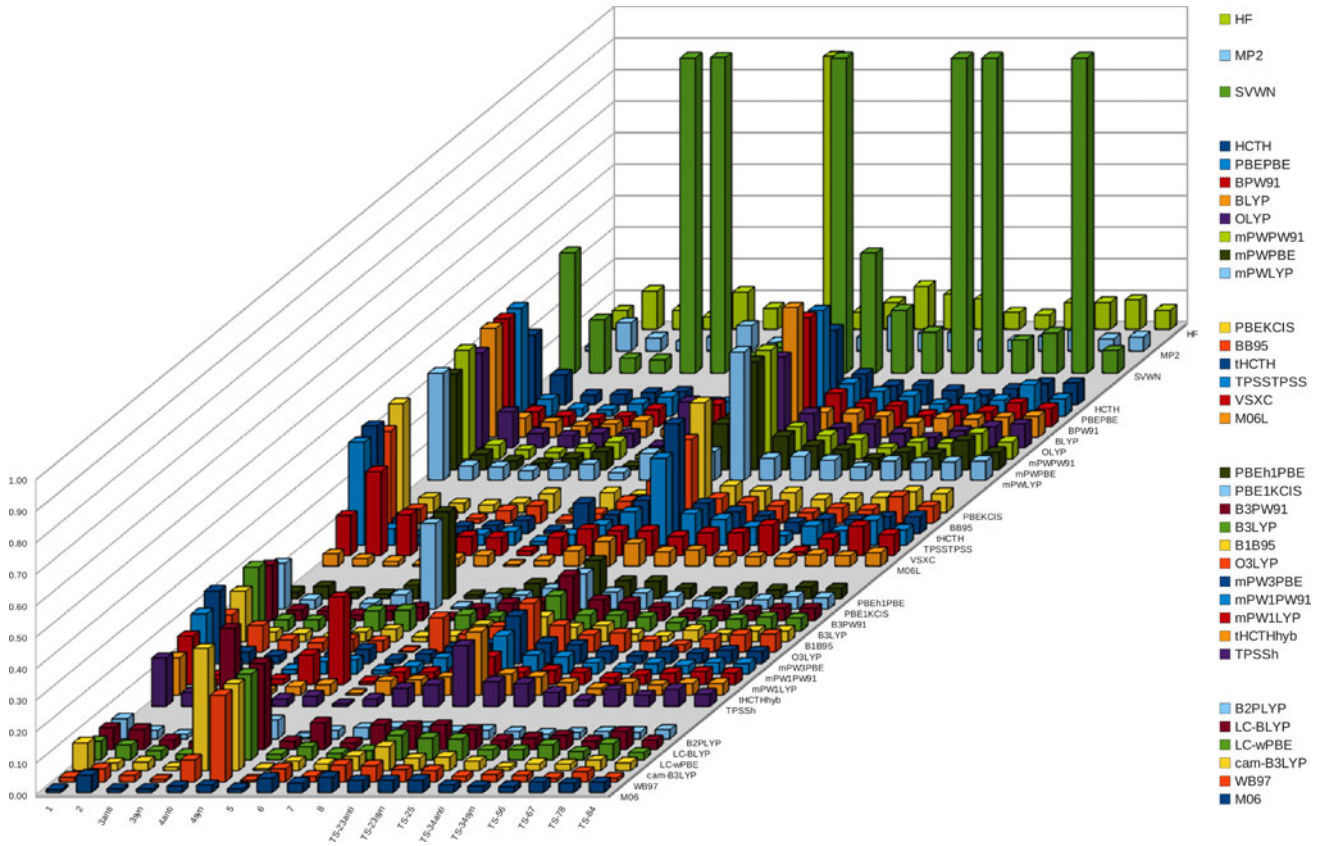


**Fig. 3** RMS values obtained after fitting the Cartesian coordinates of all computed stationary points to the CCSD reference structures (values in Å). The SVWN density functional does not describe the reaction profile accurately. Some of the stationary points cannot be located with this functional and therefore the RMS fit for them is not possible. An arbitrary RMS of 1 Å has been assigned to these structures. This value is the absolute maximum accross the functionals studied but is small enough to also avoid artifactual compression of the data range. Thus, it should be noted that a difference of a few tenths of Å with respect to these particular structures is significant

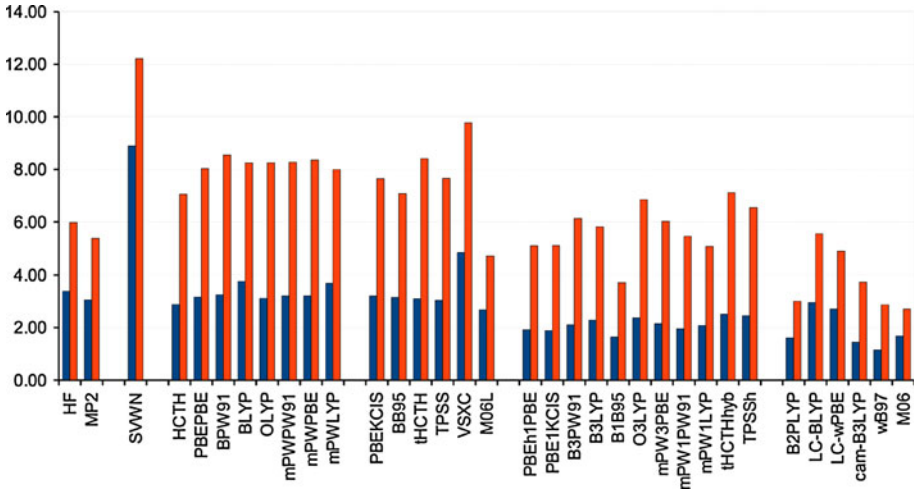


**Fig. 4** Root mean square values (RMS, in *blue*) and maximum absolute deviations (MAD, in *orange*) obtained after fitting the relative energy profiles for HF, MP2 and the 32 density functionals included in this work with respect to the energies computed at the CCSD/def2-TZVPP//CCSD/def2-SVP level (values in kcal/mol)

Figure 5 offers detailed colour-coded deviation data for the energy profiles. Analogously to what was observed in Fig. 3, there are several structures that are significantly more challenging for most functionals. As expected, among them, **TS-23-syn** and **TS-23-anti** proved to be the most difficult structures for many functionals. Errors for these transition states range within 4–6 kcal/mol for most GGA and meta-GGA functionals, decrease to 2–4 kcal/mol when exact exchange is introduced and only show values of less than 1 kcal/mol for dispersion-corrected

| | HF | MP2 | SVWN | HCTH | PBEPBE | BPW91 | BLYP | OLYP | mPWPW91 | mPWPBE | mPWLYP | PBEKCIS | BB95 | tHCTH | TPSS | VSXC | M06L |
|---|---|---|---|---|---|---|---|---|---|---|---|---|---|---|---|---|---|
| 2 | 1.35 | 2.80 | 10.58 | 7.05 | 8.03 | 8.55 | 8.24 | 8.25 | 8.27 | 8.35 | 7.99 | 7.65 | 7.07 | 8.41 | 7.66 | 0.16 | 3.26 |
| $3_{anti}$ | 3.12 | 1.36 | 0.17 | 1.94 | 0.57 | 0.97 | 3.48 | 1.42 | 0.86 | 0.58 | 3.36 | 1.63 | 1.69 | 1.29 | 0.98 | 7.54 | 3.44 |
| $3_{syn}$ | 2.75 | 0.80 | 0.07 | 2.03 | 0.63 | 1.03 | 3.55 | 1.39 | 0.90 | 0.62 | 3.41 | 1.68 | 1.64 | 1.42 | 1.03 | 7.01 | 3.40 |
| $4_{anti}$ | 5.98 | 5.37 | 10.00 | 1.56 | 0.87 | 1.28 | 2.89 | 1.79 | 1.13 | 1.00 | 2.73 | 1.19 | 0.86 | 1.49 | 1.16 | 4.48 | 1.16 |
| $4_{syn}$ | 5.84 | 5.20 | 10.00 | 1.75 | 0.84 | 1.24 | 2.97 | 2.09 | 1.11 | 0.96 | 2.86 | 1.24 | 0.83 | 1.43 | 1.13 | 4.49 | 1.21 |
| 5 | 1.45 | 0.47 | 0.27 | 3.81 | 1.93 | 2.49 | 4.55 | 3.73 | 2.22 | 2.01 | 4.27 | 3.19 | 3.60 | 2.40 | 1.99 | 9.77 | 4.72 |
| 6 | 0.32 | 4.26 | 4.69 | 0.36 | 0.85 | 0.98 | 1.29 | 0.40 | 0.99 | 1.01 | 1.33 | 0.39 | 0.50 | 1.05 | 1.03 | 3.93 | 1.31 |
| 7 | 4.13 | 2.50 | 0.82 | 1.59 | 0.30 | 0.86 | 3.26 | 1.25 | 0.65 | 0.38 | 3.05 | 1.23 | 1.28 | 1.23 | 1.02 | 6.43 | 3.24 |
| 8 | 5.42 | 4.45 | 10.00 | 0.46 | 0.06 | 0.12 | 1.51 | 0.56 | 0.09 | 0.01 | 1.48 | 0.18 | 0.08 | 0.18 | 0.11 | 5.62 | 0.85 |
| $ts23_{anti}$ | 2.56 | 3.10 | 7.62 | 0.30 | 2.06 | 1.71 | 1.26 | 0.94 | 1.93 | 2.02 | 1.52 | 1.34 | 1.11 | 1.29 | 1.90 | 2.08 | 0.95 |
| $ts23_{syn}$ | 1.18 | 0.71 | 4.01 | 1.06 | 0.55 | 0.49 | 0.92 | 0.74 | 0.52 | 0.44 | 0.95 | 1.19 | 1.11 | 0.67 | 0.12 | 1.75 | 2.34 |
| ts25 | 0.16 | 0.01 | 8.17 | 2.80 | 3.12 | 3.01 | 2.44 | 3.22 | 3.04 | 3.13 | 2.49 | 2.91 | 2.56 | 2.66 | 2.39 | 2.54 | 1.06 |
| $ts34_{anti}$ | 2.05 | 0.42 | 10.00 | 4.43 | 5.56 | 5.70 | 6.19 | 4.94 | 5.66 | 5.63 | 6.17 | 5.51 | 5.50 | 5.20 | 5.58 | 5.21 | 3.57 |
| $ts34_{syn}$ | 2.04 | 0.47 | 10.00 | 4.57 | 5.63 | 5.74 | 6.17 | 5.21 | 5.72 | 5.71 | 6.17 | 5.59 | 5.58 | 5.21 | 5.61 | 4.80 | 3.59 |
| ts56 | 1.08 | 1.07 | 1.79 | 2.45 | 2.31 | 2.29 | 2.29 | 1.94 | 2.27 | 2.23 | 2.26 | 2.35 | 2.46 | 2.54 | 2.57 | 0.02 | 2.38 |
| ts67 | 5.57 | 5.08 | 0.74 | 2.73 | 3.11 | 3.03 | 2.88 | 2.58 | 3.04 | 3.04 | 2.90 | 3.53 | 3.40 | 2.79 | 2.25 | 1.44 | 2.56 |
| ts78 | 0.58 | 0.56 | 10.00 | 1.76 | 2.16 | 2.29 | 3.12 | 2.05 | 2.28 | 2.21 | 3.14 | 2.29 | 2.29 | 2.03 | 2.26 | 4.90 | 1.92 |
| ts84 | 4.45 | 4.38 | 12.21 | 1.62 | 3.47 | 2.60 | 0.87 | 1.29 | 2.96 | 3.11 | 1.23 | 3.04 | 3.66 | 1.80 | 2.80 | 1.08 | 2.71 |

| | PBEh1PBE | PBE1KCIS | B3PW91 | B3LYP | B1B95 | O3LYP | mPW3PBE | mPW1PW91 | mPW1LYP | tHCTHhyb | TPSSh | B2PLYP | LC-BLYP | LC-wPBE | cam-B3LYP | wB97 | M06 |
|---|---|---|---|---|---|---|---|---|---|---|---|---|---|---|---|---|---|
| 2 | 5.09 | 5.10 | 6.13 | 5.81 | 3.71 | 6.84 | 6.02 | 5.45 | 5.07 | 7.11 | 6.54 | 3.00 | 1.06 | 1.43 | 3.72 | 0.71 | 2.31 |
| $3_{anti}$ | 1.02 | 0.21 | 0.56 | 1.57 | 0.68 | 0.46 | 0.88 | 1.09 | 1.62 | 0.36 | 0.19 | 1.14 | 4.94 | 4.54 | 0.86 | 1.41 | 2.12 |
| $3_{syn}$ | 1.09 | 0.27 | 0.60 | 1.53 | 0.87 | 0.39 | 0.93 | 1.17 | 1.54 | 0.41 | 0.18 | 0.94 | 5.31 | 4.89 | 1.06 | 1.70 | 1.96 |
| $4_{anti}$ | 0.02 | 0.30 | 0.49 | 1.95 | 0.34 | 1.27 | 0.24 | 0.18 | 2.08 | 1.33 | 0.69 | 2.91 | 1.64 | 2.27 | 0.68 | 0.42 | 1.11 |
| $4_{syn}$ | 0.07 | 0.30 | 0.50 | 2.06 | 0.32 | 1.55 | 0.27 | 0.20 | 2.30 | 1.26 | 0.69 | 3.00 | 1.43 | 2.22 | 0.84 | 0.43 | 1.03 |
| 5 | 0.70 | 0.60 | 0.11 | 1.88 | 0.16 | 2.09 | 0.27 | 0.66 | 1.64 | 0.86 | 0.88 | 0.48 | 5.54 | 4.29 | 1.00 | 1.93 | 2.70 |
| 6 | 0.58 | 0.13 | 0.84 | 1.14 | 0.95 | 0.45 | 0.86 | 0.79 | 1.19 | 1.44 | 0.91 | 1.55 | 1.55 | 0.25 | 1.45 | 0.48 | 0.08 |
| 7 | 1.15 | 0.50 | 0.61 | 1.44 | 0.96 | 0.32 | 0.99 | 1.15 | 1.47 | 0.32 | 0.24 | 1.43 | 5.10 | 4.55 | 0.95 | 1.31 | 2.05 |
| 8 | 0.83 | 0.60 | 0.55 | 0.81 | 0.95 | 0.17 | 0.70 | 0.74 | 1.05 | 0.30 | 0.30 | 1.99 | 2.13 | 2.63 | 0.26 | 0.64 | 0.58 |
| $ts23_{anti}$ | 1.29 | 0.77 | 1.18 | 0.84 | 0.85 | 0.80 | 1.40 | 1.32 | 0.96 | 1.65 | 1.54 | 1.24 | 2.10 | 1.39 | 1.34 | 1.26 | 0.05 |
| $ts23_{syn}$ | 0.14 | 0.68 | 0.12 | 0.36 | 0.55 | 0.44 | 0.09 | 0.02 | 0.29 | 0.09 | 0.02 | 0.28 | 0.12 | 0.39 | 0.29 | 0.62 | 1.67 |
| ts25 | 2.12 | 2.19 | 2.32 | 1.88 | 1.78 | 2.74 | 2.43 | 2.21 | 1.67 | 2.45 | 2.08 | 0.97 | 1.93 | 1.59 | 1.70 | 0.64 | 0.46 |
| $ts34_{anti}$ | 2.66 | 2.78 | 3.25 | 3.63 | 2.14 | 3.59 | 3.21 | 2.67 | 3.17 | 4.26 | 4.35 | 0.95 | 0.99 | 0.60 | 1.73 | 0.21 | 2.33 |
| $ts34_{syn}$ | 2.62 | 2.82 | 3.24 | 3.60 | 2.14 | 3.80 | 3.21 | 2.66 | 3.15 | 4.16 | 4.35 | 0.87 | 0.92 | 0.58 | 1.72 | 0.09 | 2.19 |
| ts56 | 1.95 | 1.89 | 1.94 | 1.97 | 1.84 | 1.79 | 1.89 | 1.83 | 1.86 | 1.92 | 2.38 | 1.44 | 0.23 | 0.44 | 1.02 | 0.86 | 1.86 |
| ts67 | 1.28 | 1.88 | 1.49 | 1.29 | 1.32 | 1.76 | 1.52 | 1.14 | 0.86 | 1.58 | 1.59 | 1.42 | 0.84 | 0.05 | 0.35 | 0.21 | 1.43 |
| ts78 | 0.39 | 0.50 | 0.75 | 1.40 | 0.14 | 1.12 | 0.71 | 0.40 | 1.23 | 1.65 | 1.49 | 0.37 | 1.59 | 1.69 | 0.11 | 0.47 | 0.92 |
| ts84 | 3.03 | 2.73 | 2.42 | 0.98 | 3.47 | 1.39 | 2.81 | 2.68 | 0.83 | 1.73 | 2.70 | 0.90 | 4.59 | 4.49 | 2.14 | 2.87 | 1.67 |

| Colour code: | ΔE < 2.00 | 2.00 < ΔE < 4.00 | 4.00 < ΔE < 8.00 | ΔE > 8.00 |
|---|---|---|---|---|

**Fig. 5** Detailed deviations of the relative energy (in kcal/mol) for each stationary point in the *golden carousel* after the RMS fitting procedure. In parallel to the statistical treatment of geometries, due to the SVWN density functional not describing the reaction profile accurately. Some of the stationary points have been assigned an arbitraty deviation of 10 kcal/mol and have been highlighted with *yellow* font colour. The non-complexed propargyl acetate reactant, 1:is not included in the relative energy fitting since the SCF energy difference between this structure and the rest of the intermediates in the catalytic cycle is too large. Including 1 in the RMS function leads to the complexation reaction between 1 → 2 overweighting the rest of the errors and thus, artifactually biassing the fitting procedure

formulations. The latter results suggest that, on top of soft normal modes, these intermediate organogold complexes do feature very delocalized electron densities, and that an accurate description of medium- and long-range interactions is critical even for small molecules. Interestingly, the reactant complex **2**, which did not imply any particular challenge in terms of geometric parameters, does show significant errors in the relative energies. Relative energies for both transition states **TS-23-syn**, **TS-23-anti** and complex **2** are fairly well described by Hartree–Fock and MP2, which emphasizes the relevance of a fraction of the exact exchange in the correct description of molecular systems like gold complexes with unsaturations (double and, more typically, triple bonds) where charge-transfer and weak interactions occur.

### 3.3 Energy refinements

Once we found a satisfactory methodology for geometry optimizations we used different models for single point energy calculations, in order to assess the pertinence of higher level energy refinements in the routine modeling of reaction mechanisms and also the performance of different basis sets and electron core potentials. In the absence of experimental data for the systems involved in this mechanism, we have performed CCSD/def2-tzvpp calculations on the CCSD/def2-svp geometries in order to set the energy values that we are going to use as a high quality reference, just short of the CCSD(T) that is considered the standard for *chemical accuracy*.

Against this set of energies, we are going to test the results of MP2 with the balanced basis sets of split valence, triple zeta valence and quadruple zeta valence of Ahlrichs et al., using both the PP and P polarization functions (the first designed for correlated treatments, and the second usually considered enough for DFT): [98] def2-svp, def2-tzvp, def2-tzvpp, def2-qzvp and def2-qzvpp. In all the calculations where no other electron core potential is used or the use of an all-electron basis set is not explicitly mentioned, we will use Andrae's ecp-60-mwb (5s5p5d6s, $L_{max} = 3$) pseudopotential for gold [45]. For the sake of comparison, we have also run single point MP2 calculations with the LANL2DZ [44] or SDD [45] pseudopotentials for gold, and Pople's 6–31+G(d) basis set for the main group atoms, and with a reduced valence-basis set with an SKBJ pseudopotential [99].

Since M06 was one of the best-performing functionals in terms of geometries and energies with a split valence base (def2-svp), we will also try the effect of larger basis sets and different electron core potentials with this

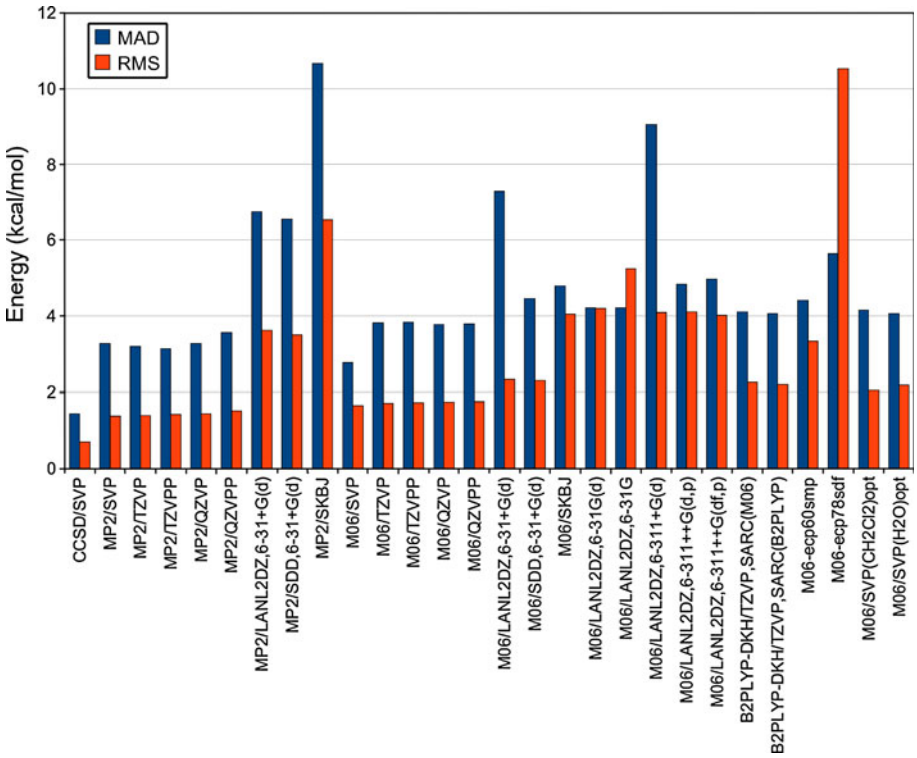


**Fig. 6** Root mean square values (RMS, in *blue*) and maximum absolute deviations (MAD, in *orange*) obtained after fitting the relative energy profiles for CCSD, MP2 and M06 single point calculations (geometry optimizations in the two series where solvation is used) on CCSD/def2-SVP geometries, with respect to the energies computed at the CCSD/def2-TZVPP//CCSD/def2-SVP level (values in kcal/mol)

functional. LANL2DZ being a popular functional in the simulation of organometallic catalytic cycles, we paid special attention to its performance with different basis sets. In this case we have chosen among Pople's basis, them being the most commonly used with it. The basis used are 6–31G, 6–31G(d), 6–311+G(d), 6–311++G(d,p) and 6–311G++(df,p).

A small deviation in the methodology, centered in gas-phase calculations, is made to take into account the effect of solvation in the energy profiles. Thus, we have used the Polarizable Continuum Model (PCM) with the integral equation formalism variant (IEFPCM) [100, 101] and UFF radii to model bulk solvent surrounding a cavity where the solute is placed. We have used dichloromethane as solvent, as it is a common choice for these reactions, but we have also used water, even if it wouldn't be compatible with the studied set of reactions, as a sort of higher bound for solvent effects modeled with continuum methods due to its high dielectric constant. Thus, the entries referring to energies or geometries in water or dichloromethane correspond to M06/def2-svp,ecp-60-mwb geometry optimizations with PCM.

An analogous approach to that followed with the DFT profiles was used to align the energy profiles (obtained taking complex **2** as the origin of energies for the mechanism) for the reactions in the general scheme minimizing their RMS with respect to the CCSD/def2-tzvpp//CCSD/def2-svp reference profile.

The results of these calculations are summarized in Fig. 6 and the fact that the best results are obtained for CCSD/def2-svp is not surprising. A quick overview of the plot highlights the good results obtained by M06, even with a relatively small split-valence basis set. Larger basis sets don't produce appreciable changes in the energies, their use even resulting in slightly larger RMS for the global profiles. This can be an effect of the design of M06, which was built against the training dataset of non-covalent interactions using the 6–31+G(d,p) basis set. These relatively small RMS and MAD values for M06 (ranging from 1.6 to 1.8 kcal/mol the RMS and from 2.8 to 3.9 kcal/mol the MAD), indicate that high-level energy refinements might not be needed for routine calculations of reaction mechanisms if the geometries are optimized at the M06/def2-svp level with the ecp-60-mwb pseudopotential. MP2 also produces good results with Weigend's basis sets, and, as found with M06, generates slightly larger RMS with larger basis. The lack of convergence in the absolute electronic energies with increasing basis size attests the non-variational nature of the method. The difference between the ranges of RMS and MAD values with MP2 (1.4–1.5 and 3.1–3.6 kcal/mol, respectively) and M06, which slightly favors the former, does not justify the extra computational cost of the perturbative method. The fact that some structures (**4**, **8** and **ts78**) in a first run display small internal wavefunction instabilities also suggests that HF might not be a good basis to build upon, reinforcing this preference for DFT methods over MP2.

The performance of other electron core potentials, such as LANL2DZ or SDD, even with larger basis sets is worse than for the ecp-60-mwb, with RMS values between 4 and 5.2 kcal/mol, with SDD leading to somewhat smaller RMS than LANL2DZ.

The most remarkable feature from this plot is the fact that the profiles in solution barely change with respect to the gas-phase reference, with a RMS(MAD) of 2.0(4.2) kcal/mol for dichloromethane and 2.2(4.1) kcal/mol for water. The fact that even in a highly polar solvent, such as water, the energy profiles are very similar to those in gas-phase, points towards the conclusion that solvent-effects, at least those that can retrieved by using a continuum approach such as PCM, are not very important in the carrousel-related part of the gold-catalyzed reactions of propargyl esters. Of special importance to those doing routine calculations with standard protocols not calibrated for each singular system is the fact that the error introduced by a non-optimal choice of functional, basis set or pseudopotential is much larger than the deviations introduced by the use of solvent, which highlights the need of a careful selection of the method employed.

Explicit inclusion of core electrons with relativistic effects described through the Douglas-Kroll-Hess (DKH) second order scalar relativistic model provide relative energies very similar to those obtained with the M06 density functional and the Ahlrichs series of basis sets. The new segmented all-electron relativistically contracted (SARC) basis sets allow the computation of energies with the DKH method very cost-efficiently, competing with the ECP strategies. Both ways of incorporating relativistic effects into the electronic structure calculations seem to perform comparably well. There are, however, a number of fields where the explicit description of core electrons is critical, like NMR spectroscopy or topological analysis of the electron density around heavy atoms.

For the sake of completeness, we have also carried out M06 single point calculations with the def2-SVP basis set for the main group atoms and the fully relativistic electron core potentials ecp-60-mdf [102] and ecp-78-sdf [103]. The results with ecp-60-mdf are comparable to those obtained with DKH, while those with ecp-78-sdf show significantly larger MAD and RMS values. The altered profile with ecp-78-sdf, which results in energies much higher for **ts34**, **4** or **8** and much lower for **6**, **7** and **ts67** could be attributed to the fact that the one-electron valence shell that is not described by the 78 electron core potential is too restricted to describe gold's bonding patterns in this catalytic cycle.

## 4 Conclusions

From these results, several conclusions can be drawn to assist in the proposal of a general routine method for the simulation of gold-catalyzed reactions of propargyl esters, a method that can probably be also applied to the study of other gold-catalyzed organic reactions involving the three main types of intermediates or exit points described in the gold carousel. Using CCSD energies and geometries as a reference, due to the lack of experimental results, DFT methods clearly outperform MP2. The small gain in RMS that can in some cases be obtained with MP2 is completely offset by the much larger computational cost. Accurate results for challenging intermediates are only obtained with the last generation of density functionals including corrections of the medium- and long-range interactions. Among these, M06 and B2PLYP generally outperform the rest of the hybrid alternatives. A brief incursion in other aspects of the modeling beyond the triad of model chemistry (functional)/basis/ECP was carried out, namely the introduction of solvation effects. The fact that the deviation introduced in the energy profiles by the use of PCM is of the same order or sometimes less than that resulting from variations in the ECP or basis set is a warning that careful selection of basis set and electron core potentials can be critical to achieve high accuracy. When the size of the catalytic system increases significantly, the available cost-efficient algorithms for pure density functionals might make M06L an attractive alternative. Further work on the performance of density functional theory in such conditions is underway.

**Acknowledgments** The authors are grateful to CESGA for allocation of supercomputer time. Funding from the Ministerio de Ciencia e Innovación (CTQ2009-13703) and the Xunta de Galicia (INCITE09 314 294 PR) is also gratefully acknowledged. We also thank Dr. Timothy Giese for his help with the RMS fitting code.

## References

1. Bond GC (1972) Gold Bull 5:11
2. Haruta M, Kobayashi T, Sano H, Yamada N (1987) Chem Lett 16:405
3. Hutchings GJ (1985) J Catal 96:292–295
4. Fukuda Y, Utimoto K (1991) J Org Chem 56:3729
5. Teles J, Brode S, Chabanas M (1998) Angew Chem Int Ed 37:1415
6. Hashmi A, Schwarz L, Choi JH, Frost T (2000) Angew Chem Int Ed 39:2285
7. Hashmi A, Frost T, Bats J (2000) J Am Chem Soc 122:11553
8. Yang CG, He C (2007) J Am Chem Soc 127:6966
9. Martin-Matute B, Nevado C, Cardenas JD, Echavarren AM (2003) J Am Chem Soc 125:5757
10. Nieto-Oberhuber C, Lopez S, Jimenez-Nuñez E, Echavarren AM (2006) Chem Eur J 12:5916
11. Hashmi ASK, Hutchings GJ (2006) Angew Chem Int Ed 45:7896
12. Hashmi ASK (2007) Chem Rev 107:3180
13. Jimenez-Nuñez E, Echavarren AM (2007) Chem Commun 333–346

14. Jimenez-Nuñez E, Echavarren AM (2008) Chem Rev 108:3326
15. Gorin D, Sherry B, Toste F (2008) Chem Rev 108(8):3351
16. Michelet V, Toullec PY, Genet JP (2008) Angew Chem Int Ed 47:4268
17. Soriano E, Marco-Contelles J (2009) Acc Chem Res 42(8):1026
18. Fürstner A (2009) Chem Soc Rev 38:3208
19. Lee SI, Chatani N (2009) Chem Commun 371–384
20. Shapiro N, Toste FD (2010) Synlett 10:675
21. Wang S, Zhang G, Zhang L (2010) Synlett 5:692
22. Schmidbaur H, Schier A (2008) Chem Soc Rev 37:1931
23. Schmidbaur H, Cronje S, Djordjevic B, Schuster O (2005) Chem Phys 311:151
24. Gorin F, Toste DJ (2007) Nature 446(7134):395
25. Perez A, López C, Marco-Contelles J, Faza O, Soriano E, de Lera A (2009) J Org Chem 74(8):2982
26. Zhang G, Peng Y, Cui L, Zhang L (2009) Angew Chem Int Ed 48:3112
27. Porcel S, Lopez-Carrillo V, Garcia-Yebra C, Echavarren AM (2009) Angew Chem Int Ed 47:1883
28. Fehr C, Winter B, Magpantay I (2009) Chem Eur J 15:9773
29. Fürstner A, Hannen P (2006) Chem Eur J 12:3006
30. Soriano E, Marco-Contelles J (2007) J Org Chem 72:2651
31. Pyykkö P (2004) Angew Chem Int Ed 43:4412
32. Pyykkö P (2005) Inorg Chim Acta 358:4113
33. Pyykkö P (2008) Chem Soc Rev 37:1967
34. Pernpointner M, Hashmi A (2009) J Chem Theory Comput 5(10):2717
35. Lein M, Rudolph M, Hashmi SK, Schwerdtfeger P (2010) Organometallics 29:2206
36. Cramer CJ, Truhlar DG (2009) Phys Chem Chem Phys 11:10757
37. Niu S, Hall MB (2000) Chem Rev 100:353
38. Harvey JN (2006) Annu Rep Prog Chem Sect C 102:203
39. Ziegler T, Autschbach J (2005) Chem Rev 105:2695
40. Bühl M, Reimann C, Pantazis D, Bredow T, Neese F (2008) J Chem Theory Comput 4:1449
41. Parr RG, Yang W (1989) Density functional theory of atoms and molecules. Oxford, New York
42. Becke AD (1993) J Chem Phys 98(7):5648
43. Lee C, Yang W, Parr RG (1988) Phys Rev B 37:785
44. Hay PJ, Wadt WR (1985) J Chem Phys 82:270
45. Andrae D, Häussermann U, Dolg M, Stoll H, Preuss H (1990) Theor Chim Acta 77:123
46. Pantazis DA, Chen XY, Landis CR, Neese F (2008) J Chem Theor Comput 4:908
47. Benitez D, Shapiro ND, Tkatchouk E, Wang Y, III WAG, Toste FD (2009) Nat Chem 1:482
48. Correa A, Marion N, Fensterbank L, Malacria M, Nolan S, Cavallo L (2008) Angew Chem Int Ed 47:718
49. Marion N, Nolan SP (2007) Angew Chem Int Ed 46:2750
50. Wang S, Zhang G, Zhang L (2010) Synlett 5:692
51. Mattsson A (2002) Science 298:759
52. Schultz NE, Zhao Y, Truhlar DG (2005) J Phys Chem A 109:11127
53. Schultz NE, Zhao Y, Truhlar DG (2005) J Phys Chem A 109:4388
54. Terkali S, Drummond M, Williams T, Cundari T, Wilson A (2009) J Phys Chem A 113:8607
55. Doren VV, Alsenoy CV, Geerlings P (2001) Density functional theory and its application to materials, 1st edn. American Institute of Physics, Melville
56. Vosko SH, Wilk L, Nusair M (1980) Can J Phys 58(8):1200
57. Adamo C, Barone V (1998) J Chem Phys 108(2):664
58. Zhao Y, Truhlar DG (2006) J Chem Phys 125:194101
59. Tao J, Perdew JP, Staroverov VN, Scuseria GE (2003) Phys Rev Lett 91:146401
60. Zhao Y, Truhlar DG (2008) Theor Chem Acc 120:215
61. Perdew JP, Burke K, Ernzerhof M (1996) Phys Rev Lett 77:3865
62. Voorhis TV, Scuseria GE (1998) J Chem Phys 109(2):400
63. Boese AD, Handy NC (2002) J Chem Phys 116(22):9559
64. Chai JD, Head-Gordon M (2008) J Chem Phys 128:084106
65. Perdew JP, Chevary JA, Vosko SH, Jackson KA, Pederson MR, Singh DJ, Fiolhais C (1992) Phys Rev B 46:6671
66. Yanai T, Tew D, Handy N (2004) Chem Phys Lett 393:51
67. Handy NC, Cohen AJ (2001) Mol Phys 99:403
68. Vydrov O, Scuseria G (2006) J Chem Phys 125:234109
69. Becke AD (1988) Phys Rev A 38:3098
70. Becke AD (1996) J Chem Phys 104(3):1040
71. Iikura H, Tsuneda T, Yanai T, Hirao K (2001) J Chem Phys 115:3540
72. Rey J, Savin A (1998) Int J Quantum Chem 69:581
73. Cohen AJ, Handy NC (2001) Mol Phys 99:607
74. Grimme S (2006) J Chem Phys 124:034108
75. Becke AD (1997) J Chem Phys 107:8554
76. Hamprecht F, Cohen A, Tozer DJ, Handy NC (1998) J Chem Phys 109(15):6264
77. Stephens PJ, Devlin FJ, Chabalowski CF, Frisch MJ (1994) J Phys Chem 98(45):11623
78. Adamo C, Barone V (1999) J Chem Phys 110:6158
79. Ernzerhof M, Perdew J (1998) J Chem Phys 109:3313
80. Slater JC (1974) Quantum theory of molecules and solids, vol 4: The self-consistent field for molecules and solids, vol 4. McGraw-Hill, New York
81. Kohn W, Sham L (1965) Phys Rev A 140:A1133
82. Hood R, Chou M, Williamson A, Rajagopal G, Needs R, Foulkes W (1997) Phys Rev Lett 78:3350
83. Perdew JP, Yue W (1986) Phys Rev B 33:8800
84. Becke AD, Roussel MR (1989) Phys Rev A 39:3761
85. Becke AD (1988) J Chem Phys 88(2):1053
86. Chermette H, Ciofini I, Mariotti F, Daul C (2001) J Chem Phys 114(4):1447
87. Perdew J, Ruzsinszky A, Tao J, Staroverov V, Scuseria G, Csonka G (2005) J Chem Phys 123:062201
88. Patchkovskii S, Ziegler T (2002) J Chem Phys 116:7806
89. Zhao Y, Truhlar DG (2008) Theor Chem Acc 120:215
90. Frisch MJ, Trucks GW, Schlegel HB, Scuseria GE, Robb MA, Cheeseman JR, Scalmani G, Barone V, Mennucci B, Petersson GA, Nakatsuji H, Caricato M, Li X, Hratchian HP, Izmaylov AF, Bloino J, Zheng G, Sonnenberg JL, Hada M, Ehara M, Toyota K, Fukuda R, Hasegawa J, Ishida M, Nakajima T, Honda Y, Kitao O, Nakai H, Vreven T, Montgomery JA Jr, Peralta JE, Ogliaro F, Bearpark M, Heyd JJ, Brothers E, Kudin KN, Staroverov VN, Kobayashi R, Normand J, Raghavachari K, Rendell A, Burant JC, Iyengar SS, Tomasi J, Cossi M, Rega N, Millam JM, Klene M, Knox JE, Cross JB, Bakken V, Adamo C, Jaramillo J, Gomperts R, Stratmann RE, Yazyev O, Austin AJ, Cammi R, Pomelli C, Ochterski JW, Martin RL, Morokuma K, Zakrzewski VG, Voth GA, Salvador P, Dannenberg JJ, Dapprich S, Daniels AD, Farkas, Foresman JB, Ortiz JV, Cioslowski J, Fox DJ (2009) Gaussian 09 Revision A.2. Gaussian Inc. Wallingford CT
91. Wheeler S, Houk K (2010) J Chem Theory Comput 6:395
92. Schäfer Ansgar, Horn H, Ahlrichs R (1992) J Chem Phys 97:2571
93. Andrae D, ermann UH, Dolg M, Stolll H, Preuß H (1990) Theor Chem Acc 77:123
94. Bauernschmitt R, Ahlrichs R (1996) J Chem Phys 104:9047
95. Douglas M, Kroll NM (1974) Ann Phys 82:89
96. Hess BA (1985) Phys Rev A 32(2):756
97. Gill PMW, Johnson BG, Pople JA (1993) Chem Phys Lett 209:506

98. Weigend F, Ahlrichs R (2005) Phys Chem Chem Phys 7:3297
99. Stevens WJ, Krauss M, Basch H, Jasien PG (1992) Can J Chem 70:612
100. Tomasi J, Persico M (1994) Chem Rev 94:2027
101. Tomasi J, Mennucci B, Cammi R (2005) Chem Rev 105:2999
102. Figgen D, Rauhut G, Dolg M, Stoll H (2005) Chem Phys 311:227
103. Fuentealba P, Stoll H, von Szentpály H, Schwerdtfeger P, Preuss H (1983) J Phys B At Mol Opt 16:L323